Argon Nanobubbles in Al(111): A Photoemission Study

C. Biswas, A. K. Shukla, S. Banik, and S. R. Barman*
Inter University Consortium for Department of Atomic Energy Facilities, Khandwa Road, Indore 452017, M.P., India

Aparna Chakrabarti
Laser Physics Division, Centre for Advanced Technology, Indore 452013, M.P., India
(Received 8 August 2003; published 19 March 2004)

Two fundamental manifestations of Al conduction electron response to Ar atom core hole in the final state of photoemission have been studied in implanted Ar bubbles in Al(111). Ar $2p$ binding energy and the Doniach-Šunjić asymmetry of the core-level line shape vary systematically as functions of Ar^+ implantation energy and number of ions bombarded (fluence). The observations are explained by relating the strength of Al conduction electron screening to the size of the Ar nanobubbles.

DOI: 10.1103/PhysRevLett.92.115506 PACS numbers: 61.80.Jh, 79.60.–i, 82.80.Pv

Rare gas (rg) bubbles formed in Al by ion implantation exhibit several interesting phenomena such as formation of solid Ar bubbles which are overpressurized and have a high melting temperature [1–4], formation of He bubbles with high mass densities [5], and electron interference between the Al surface and subsurface Ar bubbles [6]. Ar bubbles in Al is also an ideal system to study the response of conduction electrons in a nearly free electron metal to a core hole generated by photoemission in an inert solid bubble implanted in the metal. An estimate of the bubble size is of importance in different fields such as sputter growth of thin films, lifetime of reactor walls, electromigration failure in integrated circuits, etc. [7].

Argon bubbles in Al (Ar ↓ Al) have been studied using different techniques such as transmission electron microscopy (TEM), electron energy loss, x-ray absorption, scanning tunneling microscopy, etc. [1–6]. However, while there are many photoemission studies on physisorbed rg layers [8], x-ray photoemission (XPS) on implanted rg atoms are few. There is some early XPS and theoretical work on the decrease in core-level binding energy (BE) of the implanted rg atoms with respect to (w.r.t.) their gas phase BE [9–11]. The decrease in BE was explained by screening of the core hole by metal conduction electrons. Core hole screening is also manifested through the asymmetric core-level line shape for metals, quantified by the Doniach-Šunjić (DS) asymmetry parameter, α [12]. For Ar ↓ Al, α should be nonzero because of Al conduction electron screening, but Abbate *et al.* reported α to be zero for Ar $2p$ [13]. In this Letter, we report XPS results on Ar nanobubbles in Al, as a function of implantation conditions. Variation of Ar $2p$ BE and α is related to the strength of Al conduction electron screening, which depends on the size of the bubbles.

XPS experiments were performed using a commercial electron energy analyzer (from Specs GmbH, Berlin) and a nonmonochromatic MgK_α source at 6×10^{-11} mbar base pressure. An analyzer pass energy of 20 eV was used with a resolution of 0.9 eV. An electropolished Al(111) crystal was cleaned by the standard procedure. Ar implanted during the cleaning cycles was removed by annealing at 450 °C. This, as well as the absence of oxygen contamination, was checked by XPS before implantation. Ar^+ ions were implanted *in situ* in normal incidence geometry at an Ar pressure of 1.5×10^{-5} mbar for different durations at 75–100 °C substrate temperature. Since at this temperature Ar is not physisorbed on Al [8], the presence of the Ar $2p$ signal shows that Ar is implanted in Al. One monolayer (ML) fluence (F) is equivalent to 1.415×10^{15} atoms/cm^2 [14]. F was determined by measuring the current through the sample. The spectra have been fitted with two DS line shapes (Ar $2p_{3/2}$ and $2p_{1/2}$), convoluted with a Gaussian and a fixed instrumental resolution related Voigt function, using a least square error minimization routine based on the Levenberg-Marquardt algorithm. The peak position, intensity, α, intrinsic lifetime broadening, and Gaussian width were varied. The last three parameters were taken to be the same for both spin-orbit peaks; see Ref. [15] for details.

Ar $2p$ core-level spectra for 1 ML are shown in Fig. 1. For implantation energy (E_i) of 0.3 keV, the Ar $2p_{3/2}$ peak is at 242.3 ± 0.05 eV BE w.r.t. E_F, with a spin-orbit splitting of 2.1 ± 0.1 eV. An interesting observation in Fig. 1 is the 0.6 eV shift of the Ar $2p$ main peak between 0.3 and 3 keV. A similar shift of 0.5 eV is also observed for Ar $2s$. In contrast, the corresponding Al $2p$ spectra do not exhibit any change [15]. The spectra have been recorded for 37 different E_i (0.3 to 3 keV) and F (0.025 to 3 ML) combinations. The core-level shift is represented by ΔE_B, which is the difference of Ar $2p_{3/2}$ BE in Ar ↓ Al from that of the gas phase (248.45 eV) [16] [both w.r.t. the vacuum level of Al(111) with work function 4.2 eV]. For small E_i and F, ΔE_B is large (2.2–2.3 eV) (Fig. 2), while for large E_i and F it is small (1.4–1.5 eV). The overall variation of ΔE_B is $\approx$0.9 eV.

Ar bubbles in Al are reported to be in the solid phase at room temperature and are overpressurized to about

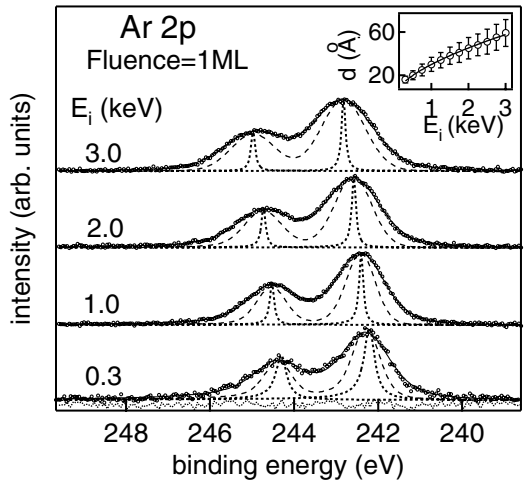

FIG. 1. Background subtracted Ar $2p$ core-level spectra (open circles) normalized to the same height and the fitted curve (thin solid line), as a function of E_i for 1 ML. The deconvoluted DS line shape (short dashes) and the spectral line shape including the Gaussian broadening but excluding the instrumental broadening (long dashes) are shown below each spectrum. The residual for the fit (for 0.3 keV spectrum) is within the experimental scatter. The inset shows the calculated projected range (d) as a function of E_i (open circles) and fitted curve (solid line); bars show the straggle.

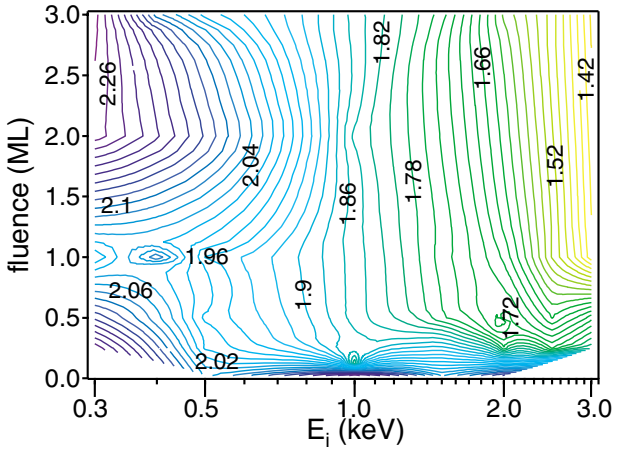

FIG. 2 (color online). ΔE_B variation as functions of E_i and F. In the gray scale (rainbow for color), the darkest (violet) contour: 2.3 eV; the lightest (yellow) contour: 1.4 eV.

60 kbar [3,4]. Hence, it is possible that the observed variation in Ar $2p$ BE might result from the compression of core electron wave functions, particularly because the radius of the bubble was found to be inversely proportional to pressure [3]. In order to examine the possible effect of pressure on ΔE_B, we have performed relativistic *ab initio* full potential linear augmented plane wave (FP-LAPW) calculations with generalized gradient approximation using the WIEN97 code [17]. Since the lattice constant of solid Ar ($a = 5.26$ Å at 4.2 K and standard pressure) has been experimentally determined as a function of pressure [18], we have performed the calculations by contracting the fcc lattice at steps of 2% to a maximum of 12% ($a = 4.629$ Å) corresponding to a pressure of $\approx$60 kbar [18]. An energy cutoff for the plane waves expansion of 13.7 Ry and $l_{\max} = 12$ has been used [15]. Between standard and 60 kbar pressure, we find a small change of 0.1 eV in Ar $2p_{3/2}$ BE; in contrast, the Ar valance band exhibits considerable shift and broadening. This is not surprising because the core-level wave functions ($2p$) are highly localized compared to the outer levels ($3s, p$). Hence, the calculated small change (0.1 eV) in Ar $2p$ core-level BE due to overpressure cannot explain the experimentally observed shift of 0.9 eV.

In previous theoretical studies on implanted rg atoms, the decrease in BE w.r.t. gas phase, i.e., ΔE_B was related to the relaxation energy (ΔE_R) [9–11]. ΔE_R arises because of the extra atomic screening by host metal conduction electrons in the final state of photoemission. ΔE_R was shown to be inversely proportional to the effective radius (R_a) of the rg atom, using a linear response relaxation model [9]. ΔE_R for Ne, Ar, Kr, and Xe are reported to be 4.8, 4.0, 3.8, and 3.5 eV, respectively [10], which varies linearly with $1/R_a$. In fact, this is a general result which can be explained by a simple image potential model, which gives ΔE_R to be $e^2/2R_a$ [11]. Thus, for Ar bubbles in Al

$$\Delta E_B = c_1/R + c_2, \tag{1}$$

where R is the average effective radius of the bubble and c_1 is the proportionality constant. c_2 represents contributions to ΔE_B which are independent of R; e.g., the physical state of Ar (since solid Ar has lower BE than gaseous Ar), the intra-atomic relaxation effect, and the electrostatic shift [9–11] (due to the dipole barriers at the Al surface and at the bubble-Al interface).

The implanted Ar atoms form bubbles because of repulsive pseudopotential and negative heat of solution of rg atoms in Al. Inglesfield and Pendry theoretically showed that it is energetically most favorable for the rare gas atoms to coalesce into bubbles [19]. Schmid *et al.* found a correlation between the number of bubbles and the amount of implanted Ar [6]. Many different experimental and theoretical studies [1–6,20,21] show that *most* of the implanted Ar atoms equilibrate into bubbles with a symmetric size distribution. For example, Rossouw *et al.* [2] report $R = 13.5 \pm 2.5$ Å for Ar $\downarrow$ Al with 50 keV and 10^{16} atoms/cm^2 fluence while, for He $\downarrow$ Al, $R = 7.5 \pm 3.0$ Å has been reported [20].

To understand how R could depend on E_i, we note that, if the projected range (d, i.e., the average depth of Ar atoms in Al) increases, a greater number of diffusion steps would be required for an Ar atom to reach the surface and desorb [22]. Since the mechanisms of bubble formation are vacancy absorption, coalescence, and emission of dislocation loops [20], for larger d the

probability that Ar atoms would absorb vacancies or coalesce would increase resulting in larger R. To find d (E_i), we have performed Monte Carlo calculations using the TRIM code [23]. d increases from 16 to 60 Å, following an empirical relation $d \propto E_i^{0.6}$ (obtained by fitting the TRIM results and is in agreement with literature [24]) (inset of Fig. 1). Hence, R should increase with E_i. Furthermore, voids formed during bombardment can act as trapping centers for Ar atoms and nucleate the formation of bubbles through absorption and coalescence. The volume of these voids can be inferred from Eq. (1) of Ref. [14] to be proportional to the energy available for nuclear collisions (E_{nuc}), which is about 92% of E_i (from TRIM calculations) in this ion energy range [15]. Hence, their radius would be approximately proportional to $E_i^{1/3}$. The above arguments indicate that R would increase with E_i, based on which we propose a relation between R and E_i: $R = c_3 E_i^n$, where c_3 is the proportionality constant and n is the exponent. Substituting this in Eq. (1), we get

$$\Delta E_B = c_1'/E_i^n + c_2. \tag{2}$$

Since ΔE_B variation with E_i is similar for different fluences above 0.025 ML, we fit these data with Eq. (2) (Fig. 3). The parameters n, $c_1'(= c_1/c_3)$, and c_2 are varied freely. The data is weighted by $1/\sigma$, where σ is the standard deviation. We obtain $n = 0.5 \pm 0.2$, $c_1' = 0.4 \pm 0.2 \times 10^{-3}$ keV$^{(n+1)}$, and $c_2 = 1.4 \pm 0.2$ eV. The value of reduced χ^2 is close to 1 (1.19), which indicates a reasonably good fit. The prediction bands show the region where the experimental data, considering random errors, would fall with 90% probability. No systematic deviation of the data from Eq. (2) is observed from the residuals. These indicate the validity of Eq. (2) in modeling the experimental data, implying that the variation of Al conduction electron screening strength related to the change in R explains the observed Ar $2p$ BE shift.

Although c_3 cannot be separately determined from the above fitting, relative variation of R with E_i can be obtained. If we assume R to be R_o for $E_i = 0.3$ keV, we find R to increase from $1.3 \pm 0.15R_o$ (for 0.5 keV) to $3.2 \pm 1.8R_o$ (for 3 keV). It should be noted that there is little change in Ar $2p$ BE in the small F region (Fig. 2). For example, for 0.025 ML ΔE_B is 2.05, 2.25, 2.05, and 2.15 eV for 0.5, 1, 1.5, and 2 keV, respectively. This is because at small F and E_i, since the implanted Ar atoms are few and far apart and d is small, the probability of coalescence to form bubbles is very small. Hence, the Ar atoms are mostly isolated and we can take $R_o \approx 1.88$ Å, which is the Ar van der Waals radius [25]. Thus, we find R (E_i) to be 2.4 ± 0.3 Å (0.5 keV), 3.4 ± 0.9 Å (1 keV), and 6 ± 3.4 Å (3 keV). Although this method of determining R is indirect and approximate, the trend is in agreement with TEM [2,3] and this further supports our explanation for the BE variation. The reported value of $R = 13.5 \pm 2.5$ Å [2] is larger than our values because of higher E_i (50 keV), F being similar [15].

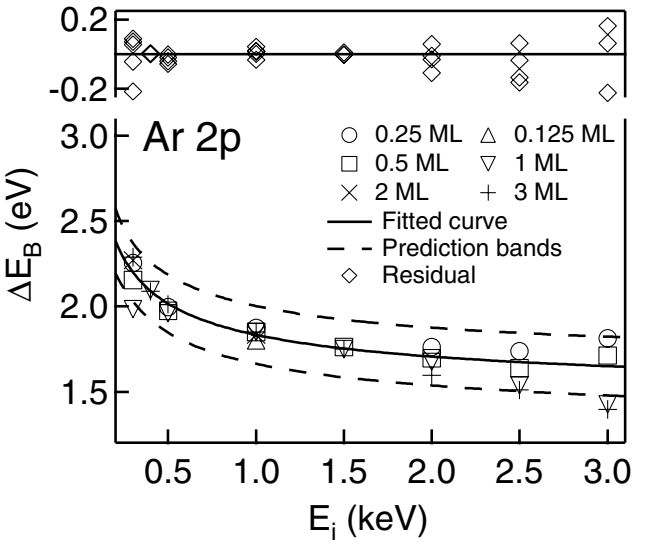

FIG. 3. ΔE_B as a function of E_i for different fluences with fitted curve (solid line) and 90% prediction bands (dashed lines). Residuals are shown at the top of the graph.

We now turn to the discussion of ΔE_B variation as a function of F. For $E_i \geq 0.5$ keV, $\Delta E_B(F)$ clearly decreases [i.e., from 2.15 eV (0.025 ML), 1.7 eV (0.5 ML), and 1.6 eV (3 ML) for 2 keV]. This decrease in ΔE_B is related to increase in bubble size with F [3]. For $E_i \leq 0.5$ keV, ΔE_B is almost unchanged as a function of F (Fig. 2); e.g., for 0.5 keV it is 2.05, 2.0, 2.0, 1.95, and 2.0 for 0.025, 0.25, 0.5, 1, and 3 ML, respectively. This is because for small E_i, desorption of the implanted Ar atoms will dominate over coalescence independent of F, since the implanted atoms can reach the surface in a lesser number of diffusion steps [22]. The decrease in ΔE_B above 0.5 keV is observed up to a certain F (0.25, 0.5, and 1 ML for 1, 1.5, and 3 keV, respectively) above which change is small. The concentration of Ar in Al in the implantation region (determined from Ar to Al $2p$ ratio considering photoemission cross sections) varies from 0.3%–0.6% for 0.025 ML to a maximum of about 3% for 3 ML. Ar concentration initially increases with F and varies little above a certain F, similar to those mentioned above. This indicates that Ar concentration reaches an equilibrium and R does not increase, which is probably why the ΔE_B change is small beyond such F.

From Fig. 1, the Gaussian width of Ar $2p$ is 0.6 eV FWHM for $E_i = 0.3$ keV, and increases to 1.2 eV for 3 keV. This substantial broadening (over and above the lifetime and instrumental broadening) arises due to the statistical distribution of bubble radii around R [2,20]. Besides, different locations of the photohole in the bubble could contribute to the width. The increase in broadening with E_i is possibly related to a larger width of R

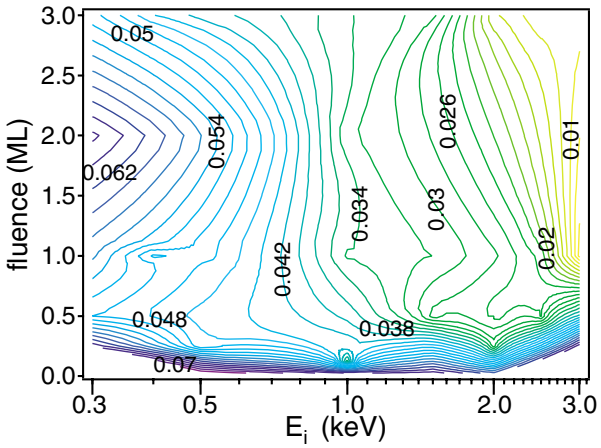

FIG. 4 (color online). α variation as functions of E_i and F. In the gray scale (rainbow for color), the darkest (violet) contour: 0.074; the lightest (yellow) contour: 0.01.

distribution, and is supported by the TRIM calculations which show larger straggle in d (inset of Fig. 1).

The screening of a core hole by conduction electrons causes infinitesimal electron-hole excitations across E_F due to the scattering of the conduction electrons by a sudden creation of the core hole. This causes an asymmetric line shape for metals, quantified by α [12]. α is related to the core hole potential (V_Q) by [26]

$$\alpha = \sum_{q<2q_F} \frac{|V_Q|^2}{|\epsilon(q,0)|^2} \frac{N(0)}{q v_F}, \qquad (3)$$

where $N(0)$ is the density of states at E_F and ϵ is the dielectric function. From FP-LAPW calculations, the band gap of solid Ar varies from 8.9 to 9.6 eV between normal and 60 kbar pressure. Hence, for solid Ar, α is expected to be zero because of the band gap. In contrast, for Ar $\downarrow$ Al, we find α to be sizable: 0.06 ± 0.007 (compare to $\alpha = 0.11$ for Al [15,16]). This is in disagreement with Ref. [13], who used the Ar $2s$ data with worse statistics for fitting [15]. We find α to vary between 0.01 to 0.06, depending on E_i and F. α is nonzero because of the Al conduction electron response to the Ar core hole potential, V_Q. There is an overall similarity in the variation of α and ΔE_B (compare Figs. 2 and 4). This demonstrates that both of these effects are related to the same physical phenomenon. In fact, it has been theoretically shown [9] that BE shift due to screening depends on the square of hole charge density, which is related to V_Q^2 on which α depends [Eq. (3)]. An asymmetry observed in Ne $1s$ for Ne implanted in Cu has been related to screening induced BE shift due to formation of Ne clusters, and the authors state that the number of these Ne clusters would increase with E_i [11]. In Ar $\downarrow$ Al, this explanation is ruled out because in that case asymmetry would increase with E_i and F. Instead, we find that, for large E_i and F, α is small (0.01) (Fig. 4), while for small E_i and F (i.e., small R), α is large (0.06). This is because for small R the Al conduction electron screening cloud is more compact, and as R increases α decreases because of reduced screening.

In conclusion, we demonstrate that Ar $2p$ BE and Doniach-Šunjić asymmetry vary systematically as functions of E_i and F due to change in Al conduction electron screening (which depends on R) in response to the Ar core hole in the photoemission final state. The variation of both BE and α with implantation conditions is similar. We show that overpressure cannot explain the observed BE shift. R is determined as a function of E_i, which might have important technological applications.

We thank Professor K. Horn, Professor V. N. Bhoraskar, Professor A. Gupta, Dr. B. A. Dasannacharya, and DST for support. Professor J. Fink is thanked for useful discussions.

*Electronic address: barman@iucindore.ernet.in

[1] A. vom Felde *et al.*, Phys. Rev. Lett. **53**, 922 (1984).
[2] C. J. Rossouw and S. E. Donnelly, Phys. Rev. Lett. **55**, 2960 (1985).
[3] J. Fink, Adv. Electron. Electron Phys. **75**, 121 (1989).
[4] G. Faraci *et al.*, Phys. Rev. B **43**, 9962 (1991).
[5] J. C. Rife *et al.*, Phys. Rev. Lett. **46**, 1220 (1981).
[6] M. Schmid *et al.*, Phys. Rev. Lett. **76**, 2298 (1996).
[7] E. Arzt *et al.*, J. Appl. Phys. **76**, 1563 (1994).
[8] T.-C. Chiang *et al.*, Phys. Rev. B **33**, 695 (1986); T. Mandel *et al.*, Phys. Rev. Lett. **55**, 1638 (1985); K. Horn *et al.*, Phys. Rev. Lett. **41**, 822 (1978).
[9] B. J. Waclawski *et al.*, Phys. Rev. Lett. **41**, 583 (1978).
[10] R. E. Watson *et al.*, Phys. Rev. B **14**, 18 (1976).
[11] P. H. Citrin and D. R. Hamann, Phys. Rev. B **10**, 4948 (1974).
[12] S. Doniach and M. Šunjić, J. Phys. C **3**, 285 (1970).
[13] M. Abbate, Phys. Rev. B **39**, 7641 (1989).
[14] C. Busse *et al.*, Phys. Rev. Lett. **85**, 326 (2000).
[15] C. Biswas *et al.* (to be published); C. Biswas *et al.*, Phys. Rev. B **67**, 165416 (2003).
[16] M. Cardona and L. Ley, *Photoemission in Solids: General Principles* (Springer-Verlag, Berlin, 1978).
[17] P. Blaha *et al.*, WIEN97, Karlheinz Schwarz, Technical Universität Wien, Austria, 1999.
[18] L. W. Finger *et al.*, Appl. Phys. Lett. **39**, 892 (1981).
[19] J. E. Inglesfield and J. B. Pendry, Philos. Mag. **34**, 205 (1976).
[20] R. Manzke *et al.*, Radiat. Eff. **78**, 327 (1983).
[21] I. Y. Goliney *et al.*, Phys. Rev. B **62**, 11 177 (2000)
[22] D. J. Reed, Radiat. Eff. **31**, 129 (1977).
[23] J. P. Biersack and L. Haggmark, Nucl. Instrum. Methods **174**, 257 (1980).
[24] J. Martan, Nucl. Instrum. Methods Phys. Res., Sect. B **2**, 202 (1984).
[25] A. Bondi, J. Phys. Chem. **68**, 441 (1964).
[26] D. C. Langreth, Phys. Rev. B **1**, 471 (1970).